Journal of Structural Geology 31 (2009) 498–511

Contents lists available at ScienceDirect

Journal of Structural Geology

journal homepage: www.elsevier.com/locate/jsg

Coeval brittle and ductile structures associated with extreme deformation partitioning in a multilayer sequence

Elena Druguet [a,*], G. Ian Alsop [b], Jordi Carreras [a]

[a] Departament de Geologia, Universitat Autònoma de Barcelona, 08193 Bellaterra (Barcelona), Spain
[b] Department of Geology and Petroleum Geology, School of Geosciences, Kings College, University of Aberdeen, Aberdeen AB24 3UE, UK

ARTICLE INFO

Article history:
Received 7 December 2008
Received in revised form
20 February 2009
Accepted 3 March 2009
Available online 13 March 2009

Keywords:
Boudin
Fold
Fracture
Multilayer rheology
Shear zone
Strain partitioning

ABSTRACT

An investigation on the effects of a strong rheological contrast in the deformation of layered anisotropic rocks is presented. The study focuses on the geometric and kinematic analysis of complex structures developed within and adjacent to a thin marble–metapsammite multilayer unit from the Cap de Creus tectonometamorphic belt (NE Spain). Zones of high ductile strain localise in the marble layers, which exhibit complex folds, whereas metapsammites show mostly brittle (boudinage) structures. These structures strongly contrast with coeval retrogressive discrete shear zones developed in the surrounding migmatitic schists. The extreme strain partitioning is due to the rheological contrast between different lithological layers. In addition, the specific orientation of this multilayer unit induces a reversal of local kinematics with regard to bulk kinematics. Consequently, caution should be exercised when interpreting regional tectonics in highly partitioned domains associated with rheological heterogeneities.

1. Introduction

Structural geologists frequently divide deformation into ductile and brittle "fields" with fractures often regarded as the opposite to folds because they are considered the type-structures of brittle and ductile deformation respectively (see textbooks e.g. Twiss and Moores, 1992; van der Pluijm and Marshak, 2004). However, simultaneously formed fractures and folds have been reported in a large variety of tectonic contexts and crustal domains not restricted to the brittle–ductile transition. The interaction between fracture and flow can be triggered by different mechanisms. One is the time fluctuation in the mechanical behaviour of deforming rocks, such as in the case of ductile shear zones that localise from precursor fractures (Fusseis et al., 2006; Mancktelow, 2008a). Another likely cause is the presence of extreme lithological heterogeneities, and this is the scope of the present work. In the upper crust, fractures are commonly associated with folds (e.g. Stearns, 1964; Suppe, 1985) and faults and folds are usually coupled in respectively brittle strata and unlithified or soft sediments in both compressional and extensional settings (Strachan and Alsop, 2006). In the mid to lower crust, which is the locus of this study, the most common situations where this may happen are summarised below and shown in Fig. 1.

(1) In rheologically layered rocks, a relatively competent layer can be subjected to simultaneous shortening and extension, folding in one direction and breaking into boudin blocks in another direction (Grujic and Mancktelow, 1995; Zulauf and Zulauf, 2005; Mancktelow, 2008b; Fig. 1a). Alternatively, a segment of the layer being folded and another segment being pulled apart may occur on a single section because the two layer segments fall into the shortening and extensional field respectively (Fig. 1b). Fractures and folds may also form in an individual layer as a result of progressive deformation (e.g. first shortening and then extension, Fig. 1c).
(2) Folds and fractures can develop in competent layers of variable initial orientation (Fig. 1d). This is typical of domains with sets of differently oriented veins or dykes which, due to their competence relative to the host rocks, become folded or boudinaged depending on their orientation with regard to the kinematic axes. They are thus suitable for strain and kinematic analysis (e.g. Hutton, 1982; Passchier, 1990; Druguet et al., 2008).
(3) Layered rocks with a strong rheological contrast may also display coeval fracturing and folding. Ductile flow is partitioned into weak layers where shearing and folding are

* Corresponding author. Fax: +34 935811263.
E-mail address: elena.druguet@uab.cat (E. Druguet).

0191-8141/$ – see front matter © 2009 Elsevier Ltd. All rights reserved.
doi:10.1016/j.jsg.2009.03.004

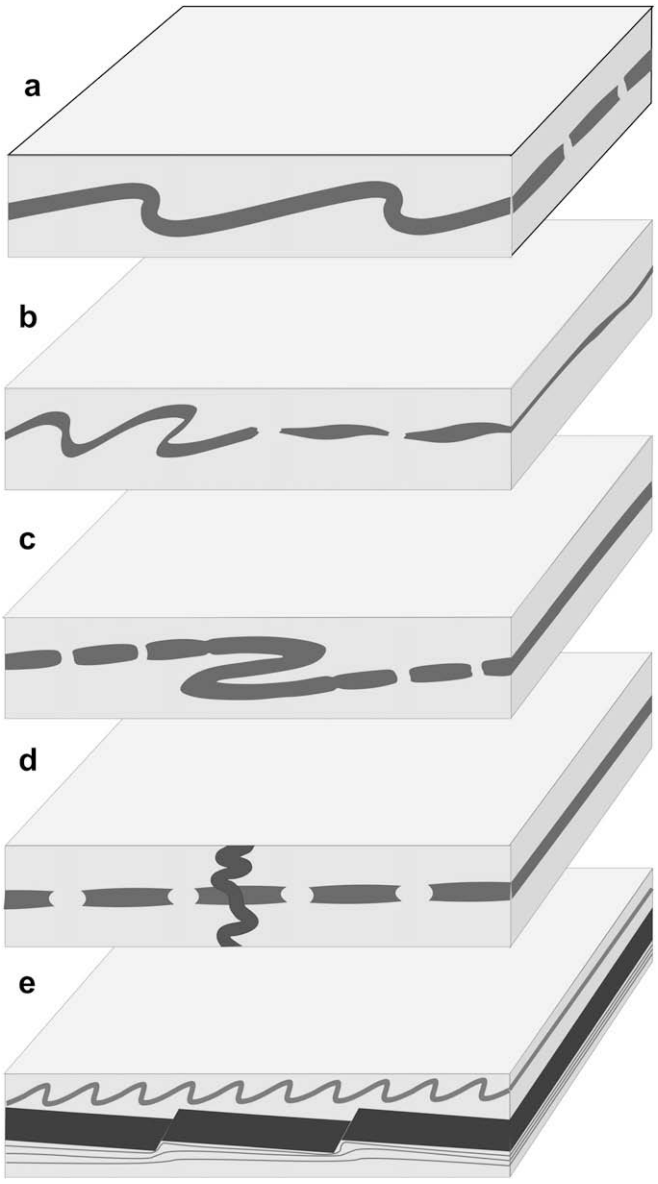

Fig. 1. Sketches of different situations in the mid crust where folding and fracturing are possible during a single deformation event. (a) A competent layer (dark grey) records simultaneous folding and fracture boudinage. (b) Simultaneously folded and boudinaged segments of a layer on the same section. (c) Progressive deformation of a folded competent layer leads to extension (boudinage) of the limb zones. (d) A discordant competent dyke folds while the competent layer is boudinaged. (e) Fracture boudinage of a brittle layer (black) embedded in much more ductile layers that deform by folding (drag and accommodation folds arbitrarily sketched above and below the brittle layer respectively).

developed, whilst layers of competent rock are dominated by brittle deformation associated with fracture boudins and faults (Fig. 1e). In these cases, accommodation folds may also form in the weak units adjacent to fractures in the strong layers (e.g. Harris et al., 2002).

The present case study includes most of the situations described above, although this work mostly concerns point (3). In this situation, an overall transpressional deformation is partitioned into a ductile simple shear dominated flow of the rheologically weak layers, coupled with a brittle failure of the strong layers. Deformation partitioning is a common feature in transpression zones (Tikoff and Teyssier, 1994; Jones and Tanner, 1995), but occurs more widely in multiphase materials under any tectonic regime. Deformation partitioning includes partition of vorticity (or non-coaxiality) between a dominantly coaxial flow of the high-viscosity phase and a non-coaxial flow of the lower-viscosity phase (e.g. Lister and Williams, 1983; Vigneresse and Tikoff, 1999; Takeda and Griera, 2006). During partitioning, the sense of vorticity in layers of contrasting viscosity may even be opposite (Ishii, 1992; Hippertt and Tohver, 1999) or may change with progressive deformation (Jiang, 1994).

In the present case study, we investigate folds and fractures affecting a series of interlayered carbonate-rich rocks and metapsammites from Cap de Creus in the eastern-most Pyrenees, Spain. Geometrical and structural analyses reveal that coeval complex folding and fracturing developed as a result of an overall single transpressional deformation. This deformation was partitioned into separate domains corresponding to highly contrasting lithological and rheological units.

2. Lithotectonic setting

The study area is located in the Tudela migmatitic complex (Druguet, 2001; Fig. 2a) of the Northern Cap de Creus peninsula. Lithologically the area consists of metasedimentary rocks with minor metaigneous intercalations (amphibolites). The protolith of this sequence, referred to as the Cadaqués series (Navidad and Carreras, 1995) is considered Neoproterozoic in age and is intruded by granitoids dated at 553 ± 4.4 Ma (Castiñeiras et al., 2008).

During the Variscan, the rocks of the Cadaqués series were affected by polyphase deformation, with three main deformation episodes (D_1–D_3) related to an overall transpressional event (Druguet, 2001). D_1 is characterized by a widespread bedding-parallel foliation. D_2 in the study area was intense and produced $a \approx 500$ m wide E–W trending zone of high strain where bedding/S_1 is transposed into a moderate to steeply dipping composite bedding/S_1/S_2 foliation (Fig. 2a and b) with a few relics of tight to isoclinal D_2 folds (Druguet and Carreras, 2006). L_2 stretching lineations are moderately to steeply plunging towards the NW (Fig. 2b). Metamorphism in the study area reached upper amphibolite facies conditions (Sil–Kfeldspar zone) during D_2 resulting in anatexis and partial migmatization of the schists around a small intrusion of tonalite and quartz-diorite. There followed the emplacement of a swarm of anatectic pegmatites (Fig. 2a; Druguet, 2001; Bons et al., 2004). Continuing transpressional deformation during retrogressive (upper greenschist) metamorphic conditions was characterized by strain localization that gave rise to a network of shears with predominantly dextral strike-slip movement. These form the classical D_3 Cap de Creus shear zones and mylonites which overprint and therefore post-date all the pre-existing structures (Carreras, 2001). Structures related to this shear zone network include folds and sheath folds (Carreras and Casas, 1987; Carreras et al., 2005; Alsop and Carreras, 2007), shear bands (White et al., 1980) and also shear fractures (Fusseis et al., 2006; Gómez-Rivas et al., 2007). The occurrence of fractures associated to mylonitic fabrics allowed Fusseis et al. (2006) and Fusseis and Handy (2008) to interpret the shear zones as developed at the brittle–viscous transition. In the study area, the D_3 shear zone network is represented by two main contemporary sets of discrete shears cutting across the migmatitic schists (Fig. 2a and c): a dominant steeply dipping N–S trending set with dextral movement, and another shallowly-dipping set associated with top-to-the-south movement.

2.1. The marble–metapsammite unit

The metasedimentary series outcropping in the studied portion of the Tudela migmatitic complex form a cm–m alternation of,

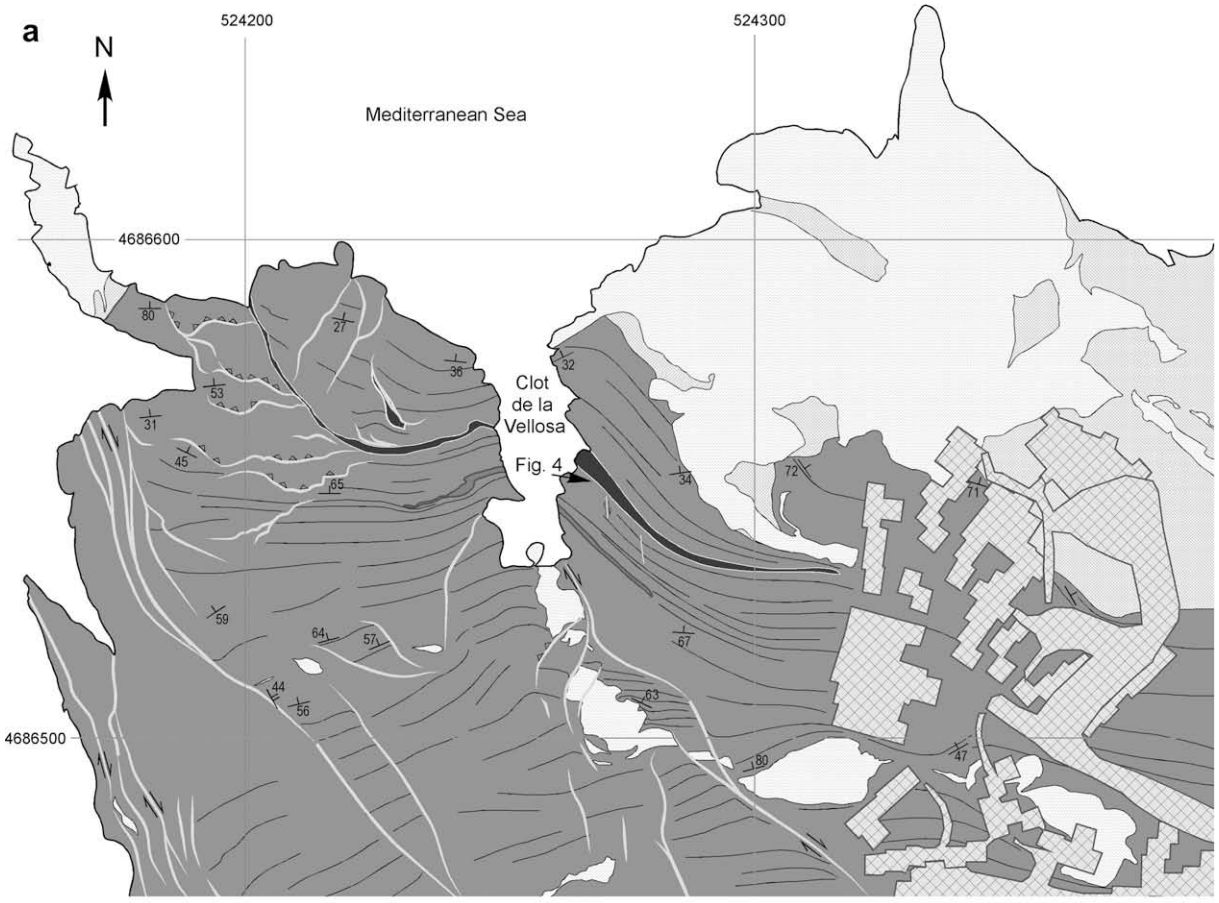

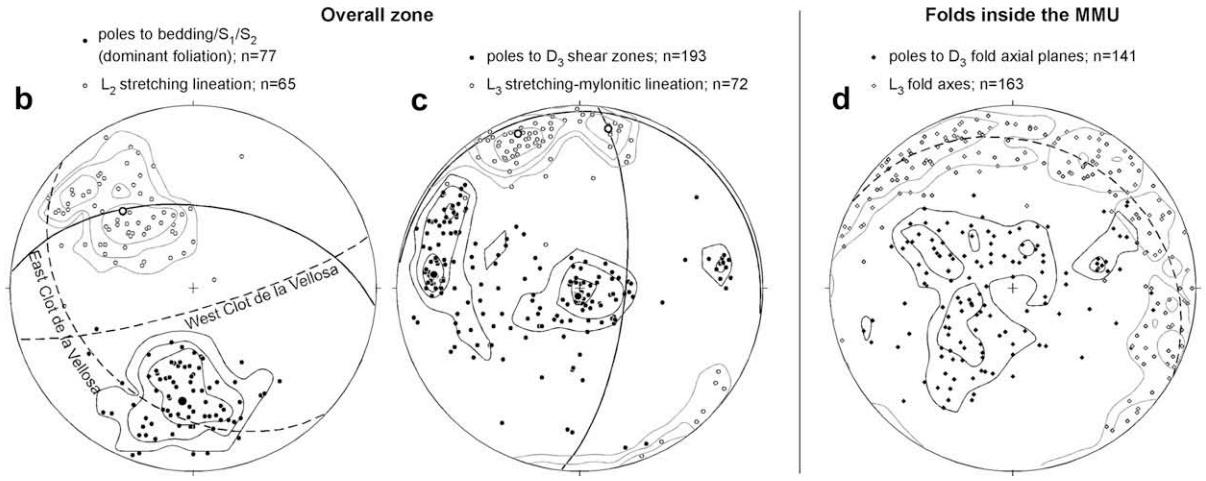

Fig. 2. (a) Litho-structural map of the study area in the Tudela migmatitic complex (NE Cap de Creus peninsula). (b)–(d) Lower hemisphere equal area stereoplots of structural elements in the study area. (b) Poles to bedding/S_1/S_2 and L_2 stretching lineation (contour intervals: 2%, 4%, 8%). The mean foliation plane is depicted with a solid great circle. Dashed circles are MMU exposure surfaces. (c) Poles to D_3 shear zones (contour intervals: 2%, 4%, 8%) and L_3 mylonitic lineation (contour intervals: 2%, 4%, 8%, 16%). The mean planes of the two sets of shear zones are depicted with solid great circles. (d) Poles to D_3 fold axial planes and L_3 fold axes inside the MMU (contour intervals: 2%, 4%). The dashed great circle is the fold axis girdle.

partly migmatitic, sillimanite bearing schists (metapsammites and metapelites). East and west of a small bay called Clot de la Vellosa (Fig. 2a), a distinct, 1–3 m thick, lithologically complex multilayer unit is directly traceable for 120 m as a zone within this metasedimentary series. This distinct unit comprises metacarbonates (mostly calcareous marbles with variable amounts of impurities and variable texture from laminar to brecciated), calc-silicate rocks, metapsammites (metagreywackes and quartzites) and graphitic schists; this sequence is hereafter referred to as the marble–metapsammite unit (MMU). Elsewhere in the north Cap de Creus peninsula it is occasionally present and referred to as the Sant Baldiri unit (Carreras and Ramírez, 1984). The similarity of this unit with rocks of the series overlaying the Cadaqués series, together with its discontinuous and irregular appearance within the Cadaqués series, suggest that the MMU may represent tectonic slices related to D_1 thrusting (Druguet, 1997). The fact that the MMU in the study area becomes thinner eastwards (Fig. 2a) can be attributed to D_1, but also to D_2 tight folding and transposition.

An idealized "rheological" profile across the MMU is qualitatively represented in Fig. 3a, with the relative competence between different lithologies depicted in grey-scale. The hereafter termed competence contrast, as described in Ramsay (1982), will refer to the finite effective viscosity ratio quantitatively or qualitatively estimated for field structures. Such competence contrasts were inferred from structures and fabrics observed in each rock type. Four main lithotypes have been distinguished from more to less competent (lighter to darker):

(1) Metapsammites: grouped under this name are foliated (S_1/S_2) biotite–sillimanite paragneisses interbanded with minor schistose selvages, quartz–feldspar lenses (migmatitic leucosomes) and plagioclase–amphibole gneisses.
(2) Calc-silicate rocks with granoblastic to weak gneissic D_2 fabric.
(3) Migmatitic schists: they form the dominant lithology in the area (wall rock of the MMU) and consist of banded migmatites made of alternating metapsammites and metapelites together with leucocratic veins and lenses (described in Druguet and Carreras, 2006).
(4) Marbles: grouped under this name are ±impure metacarbonates. Two main textural types can be distinguished, a ±homogeneous dark marble with fragments of metapelite, calc-silicate rocks and quartz (marble breccia) and a white–grey banded marble, where banding is defined by the alternation of carbonate-rich zones with metapelite and calc-silicate laminae. Both textural types are common elsewhere from low- to high-grade metamorphic zones in the northern Cap de Creus where this unit outcrops and, thus, they are likely due to original lithological heterogeneities and D_1 tectonic brecciation.

Retrogression of the high-temperature assemblages and associated fabrics to those typical of greenschist-facies conditions is minor and restricted to localised areas in the strongly deformed marbles, as indicated by the presence of epidote and chloritized interlayered metapelites. Various deformed quartz and leucogranite veins are also present in the area (Fig. 4), although they are not the object of our current investigation and are not described further here.

For a better assessment of competence contrast between different rocks of the MMU, we have applied the technique of Schmalholz and Podladchikov (2001) which estimates strain and competence contrast directly from fold shapes. We measured the relationships between fold amplitude (A), fold wavelength (λ) and thickness (H) from twenty-fold profiles and plotted them on a strain contour map (Fig. 3b). In order to be able to apply the method, which considers single layer folds in an isotropic medium, most fold measurements were made on widely spaced layers embedded in thicker low anisotropic marble; Schmid and Podladchikov (2006) showed that if the interlayer spacing is large, individual layers behave and fold as single layers. However, in the case of some

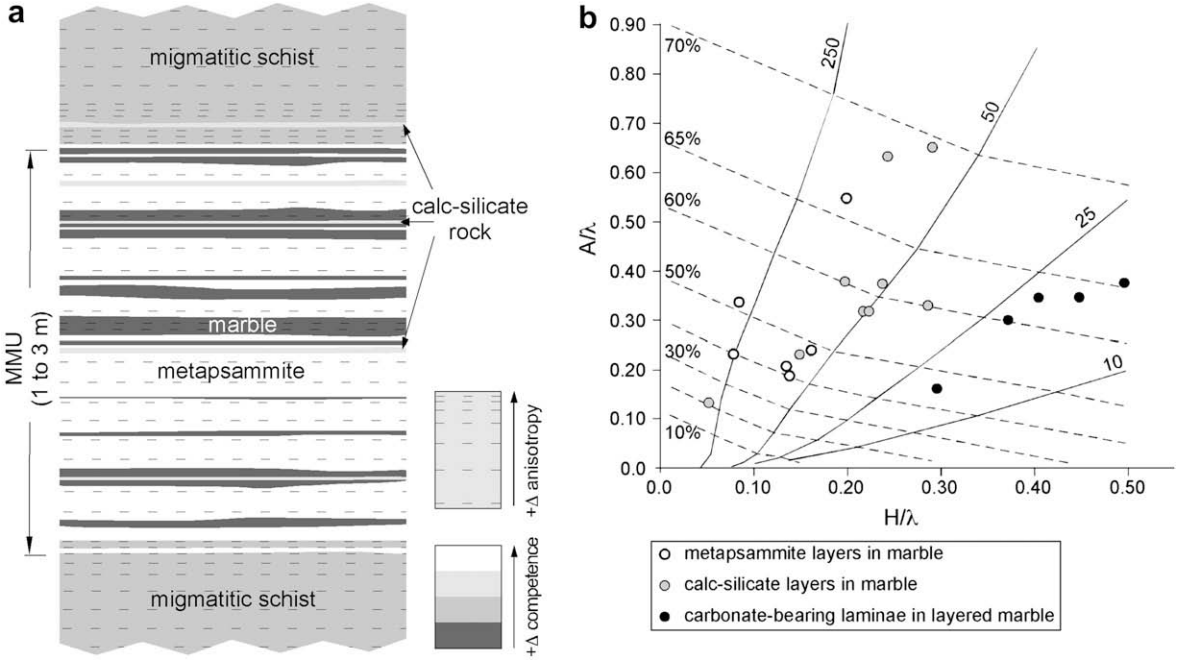

Fig. 3. (a) Schematic type section of the MMU. (b) Ratios of A/λ and H/λ from measured fold profiles plotted in the strain contour map of Schmalholz and Podladchikov (2001). Plain lines mark competence contrasts of 250, 50, 25 and 10. Dashed lines are contours of layer shortening in percent.

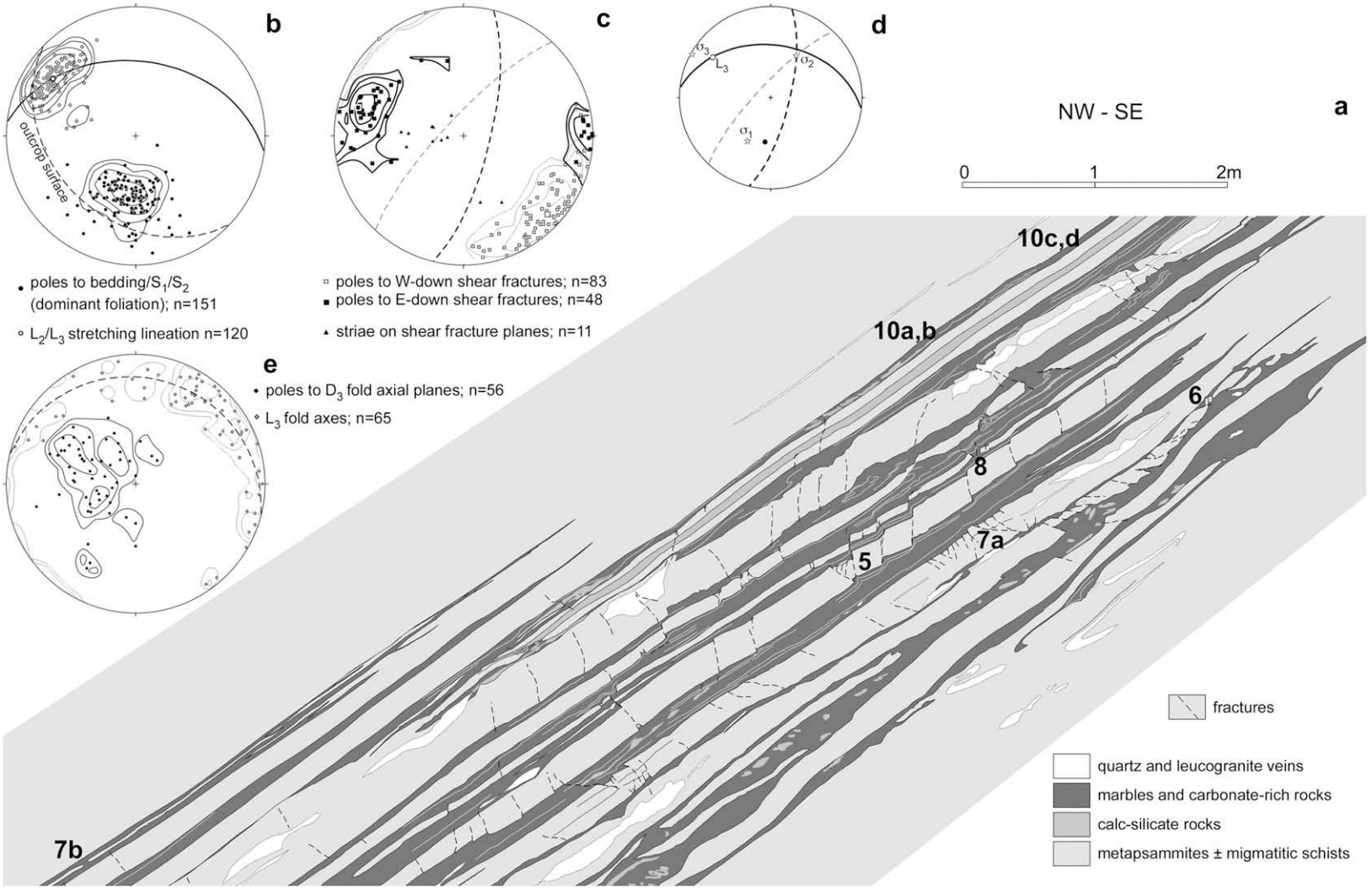

Fig. 4. (a) Detail litho-structural section along the eastern slope of Clot de la Vellosa. The structure was drawn in the field on a set of photo-maps with each one corresponding to an area of 2 × 2 m, assembled from photographs taken from the opposite side of the bay. (b)–(e) Lower hemisphere equal area stereoplots of structural elements from this section. (b) Poles to bedding/S_1/S_2 (contour intervals: 2%, 4%, 8%, 16%, 32%) and L_2/L_3 stretching lineation (contour intervals: 2%, 4%, 8%, 16%). The mean foliation plane is depicted with a solid great circle. Dashed circle is the east Clot de la Vellosa outcrop surface. (c) Poles to shear fractures (contour intervals: 2%, 4%, 8%) and fault striae. The dashed grey and black great circles are the mean planes of the W-down and E-down sets respectively. (d) Plot of the deduced local stress field in the brittle layers compared to the mean foliation and L_3 stretching lineation. (e) Poles to D_3 fold axial planes and L_3 fold axes (contour intervals: 2%, 4%, 8%). The dashed great circle is the fold axes girdle.

carbonate laminae, the values are likely to be overestimates, since the measured folds inside the layered marbles correspond more to a multilayer folding mechanism which will effectively increase fold amplification rates. The metapsammite and calc-silicate layers give large values of competence contrast with respect to the embedding marbles. The metapsammites are the more competent (with an average competence contrast of ≈ 100), whilst carbonate-bearing layers interlayered with relatively softer marbles give much lower values (mean competence contrast of ≈ 18).

The variations in the degree of anisotropy between different lithologies are also illustrated in Fig. 3a, based on the degree of schistosity in the silicate rocks and the internal lamination in the metacarbonate rocks.

3. Structural and kinematic analysis

Inside the MMU, fractures and boudins are prevalent in the metapsammites, whereas folds are more widespread in the marbles. Fractures, boudins and folds are interpreted as D_3 structures because most of them overprint the high-temperature D_2 fabrics, and some fractures can be traced outside the MMU directly into D_3 shear zones. These complex features contrast strongly with the relatively simple structures observed in the embedding schists, which are characterized by the presence of a sole, penetrative E–W trending D_2 foliation locally cut by discrete D_3 shear zones (Fig. 2a).

We now describe and analyse the complex deformation structures developed within and at the margins of the marble–metapsammite unit. Observations were made on three main exposure surfaces along the MMU, located east and west of Clot de la Vellosa (Fig. 2a and b). The internal and marginal structures will be analysed separately.

3.1. Structures developed within the marble–metapsammite unit

The structural pattern within the MMU is characterized by an association of fractures and buckle folds in the competent layers, together with ductile D_3 fabrics and complex folding in the incompetent rocks. An S_3 foliation is only developed in the metacarbonates, defined by the preferred orientation of mineral aggregates and clasts. It trends sub-parallel to the axial planes of the tight F_3 folds and at a small angle to the dominant bedding/S_1/S_2 fabric. The direction of maximum extension and transport during D_3 is marked by a shallow plunging L_3 stretching lineation (Fig. 4), well defined by a ridge-and-groove type lineation (Lin et al., 2007) on the interface between metapsammites or calc-silicate rocks and marbles. This L_3 lineation is inherited from the earlier D_2 event, having been rotated from steeper into shallower orientations (compare stereoplot in Fig. 2b with that in Fig. 4). A new L_3 is developed only in lithologies such as quartz pods that had no foliation and lineation prior to D_3. The obliquity between S_3 and bedding/S_1/S_2, and the orientation of L_3 allows shear sense to be interpreted as sinistral with a minor normal (top-to-the-north) component. This contrasts with the previously mentioned prevalent dextral sense of the shear zone network.

3.1.1. Structures related to layer-parallel extension

Extensional structures are best observed in outcrops oriented sub-parallel to the extension direction, as developed on the eastern slope of Clot de la Vellosa (Figs. 2 and 4). Shear fractures or faults are abundant in the competent layers and imply layer-parallel extension. Normal fault geometries apply when considering the layering as the reference plane, although if we consider the modern geographical reference frame some of the faults have passed through the vertical and now display an apparent reverse slip motion (Fig. 4).

There are two distinct sets of conjugate shear fractures according to the sense of slip, a W-down and an E-down set (Figs. 4–7a). Most of these affect the competent metapsammites, but also some layers of calc-silicate rock and amphibolite and quartz or quartz-feldspathic veins are fractured. Fault striae are scarce but well defined, indicating dip-slip motion for the W-down set and oblique-slip motion for the E-down set (Fig. 4). The angle between the two fracture sets is $\approx 43^\circ$ and their bisector plane is at a large angle (75–80°) to the main layering/foliation. The W-down and the E-down sets display synthetic- and antithetic-slip respectively when compared with the bulk layer-parallel sinistral–normal movement deduced for the MMU.

Asymmetric fracture boudinage structures are developed where any of the two fracture sets cut an entire competent layer (Figs. 5 and 6). When the layer is enclosed in incompetent marble, the fracture may propagate as a shear band at the margin of the layer into the enclosing incompetent marbles. However, more typically the fracture terminates and displacement along interboudin fractures and rotation of boudin blocks are accommodated in the incompetent host by ductile flow and folding of marble layers (accommodation folds, Figs. 1e and 5). Such accommodation folds are good examples of brittle–ductile coupling associated with extreme strain partitioning at the meso-scale. The rigid behaviour of boudins and the lack of evidence for D_3 ductile deformation (elongation or development of barrel-boudins) are in agreement with the high competence contrast between metapsammites and marbles. Boudins are rotated with respect to the enveloping layer by different amounts but, usually, the lower the aspect ratio the greater the rotation. This is well illustrated in Fig. 6 where boudins with the lowest aspect ratio are rotated with a top-to-the-NW sense by up to 45°. Interlayer slip may also take place on these highly rotated boudins consistent with the bulk layer-parallel sinistral–normal flow, and this is responsible for further layer segmentation (Fig. 6). Restoration of fractured layers allows appraisal of their initial shape, and the amount of layer-parallel extension. The reconstruction performed in Fig. 6 reveals that some layer necking had occurred before fracturing. Such early necking of competent layers is also noticeable along the thickest layers depicted in Fig. 4, and, assuming D_2 tight folding and transposition, the necking could correspond to the stretching (pinch-and-swelling) of fold limbs during D_2 isoclinal folding. It is also important to note that, despite the pronounced local degrees of offset and rotation, the stretch value estimated from the boudin train is rather low ($S = 1.1$; 110% layer-parallel extension) (Fig. 6).

In relatively thick (>35 cm) competent layers, shear fracturing did not propagate through the entire layer and does not therefore lead to boudinage. Conjugate shear fractures instead develop small horst-and-graben arrays on the layer walls (Figs. 4 and 7a). Again, displacement along small faults and rigid rotation of blocks are accommodated by ductile flow of the enclosing marbles. At the metric scale (Fig. 4), these horst-and-graben arrays are preferentially located within necked zones of the thick competent layers.

In relatively thin (<10 cm) competent layers, the fracture type is completely different to that described above. In this case, extension fracture boudinage (due to mode I tensile fracturing) is the dominant process (Fig. 7b). The resulting boudins have rectangular shapes marked by extension fractures at high angles to layering. In many cases, adjacent boudins are oblique to one another and have rotated or curved edges that may even converge (Figs. 7 and 8a). The interboudin zone typically appears as a graben delimited by conjugate normal faults. Our suggested mechanism is that mode I extension cracks would have initiated and propagated as wedge-shaped cracks (Fig. 8b). Interboudin gaps are always filled with the hosting carbonate.

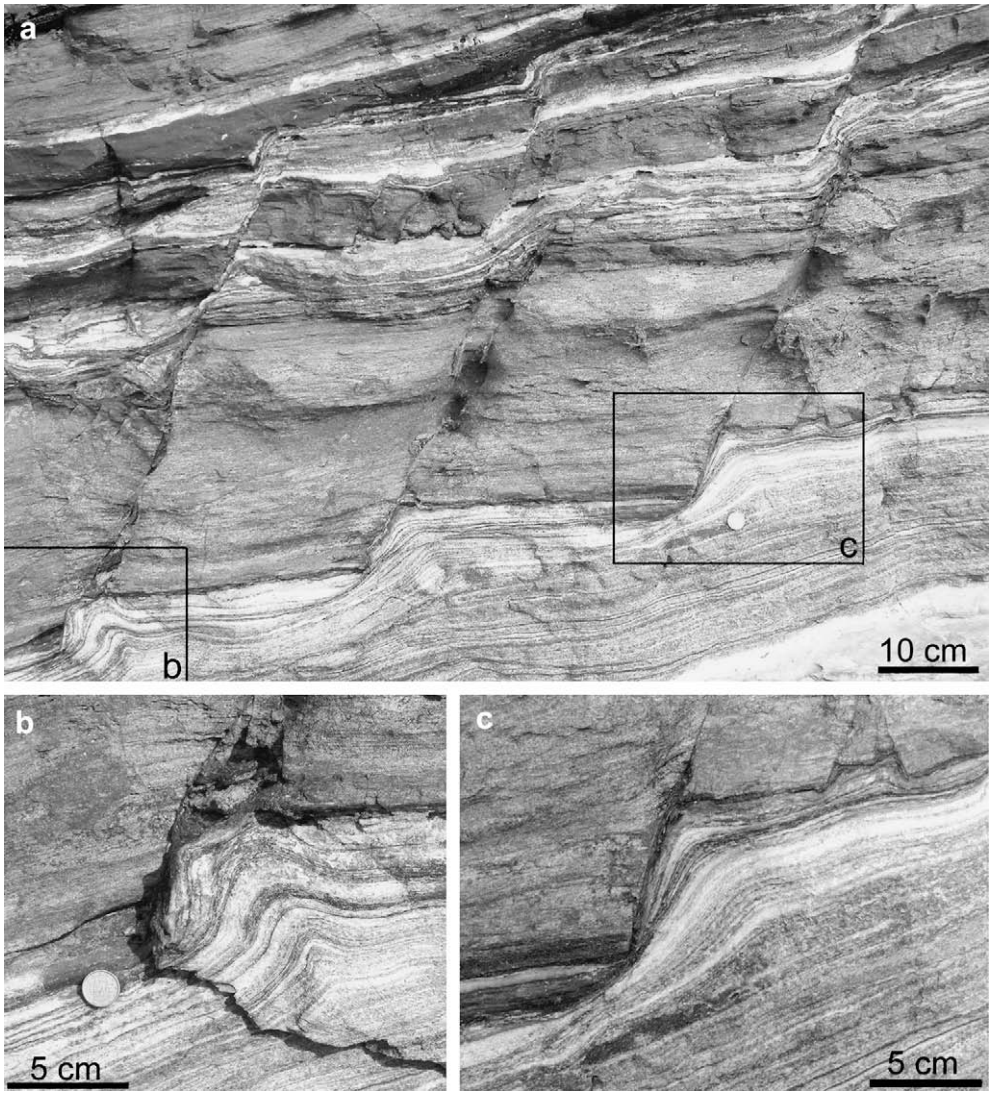

Fig. 5. (a) Boudinaged metapsammite and calc-silicate layers. Asymmetric boudins are delimited by a W-down set of fractures. The interlayered marbles accommodate the slip along fractures by ductile flow. (b), (c) Details of the accommodation folds developed in the marble next to the sharp boudin corners. Two conjugate small faults are also shown in (c). The measured stretch of this boudin train is $S = 1.1$. See Fig. 4 for location of the photographs.

More complex structures result from the combination of wedge-shaped extension fracture boudinage and formation of subsidiary shear fractures (Fig. 8b). This interaction between extension and shear fractures has been tested with analogue experiments using the BCN-Stage (Druguet and Carreras, 2006). A multilayer made of alternating competent layers of plasticine (grey) and incompetent layers of plasticine with 9% wt. vaseline (white) was subjected to layer-normal compression. A sequence of four deformation stages in a portion of the model is shown in Fig. 8c. First, a wedge-shaped extension crack formed in the competent layer. Subsequent rotation of the layer segments adjacent to the crack triggered the formation of conjugate shears. Contemporary extension and shear fractures are often observed in nature and experiments, particularly in sequences with a rheological layering (Peacock and Sanderson, 1992; Ghosh, 1994; Schöpfer et al., 2006). Healy et al. (2006) show with numerical models of isotropic brittle media that shear fractures can form by the coalescence of interacting mode I cracks.

The mode of fracturing of brittle layers embedded in ductile layers depends not only on the competence contrast between layers (Peacock and Sanderson, 1992), but also on the thickness ratio of brittle and ductile layers in the multilayer (T_r), as already theoretically predicted and experimentally demonstrated by Mandal et al. (2000). This is because the stresses on the brittle layer are transferred from the ductile matrix, and hence are controlled by the thickness ratio (Ramberg, 1955; Mandal et al., 2000). Our natural case study, which represents a multilayer system with a given (fixed) high competence contrast, demonstrates the dependence of fracture mode on the thickness ratio. In this case, extension fracture boudinage (rectangular boudins) generally occurs when $T_r < 1$ and shear fracture boudinage (asymmetric boudins) occurs when $T_r > 1$ (Fig. 9). An intermediate field around $0.5 < T_r < 1.5$ would be represented by those situations involving a complex interaction between extension and shear fractures (e.g. Fig. 8). For $T_r > 4$ (not represented in the graph) shear fractures develop, but only on the outer areas of the competent layers, giving rise to horst-and-graben domains (e.g. Fig. 7a). In our case, extension fracture boudins have variable aspect ratios ranging between 1 and 10, whereas shear fracture boudins have $A_r < 2$. Mandal et al. (2000) also theoretically predicted that the aspect ratio of boudins (A_r) is inversely proportional to T_r (negative slope of the curve in Fig. 9).

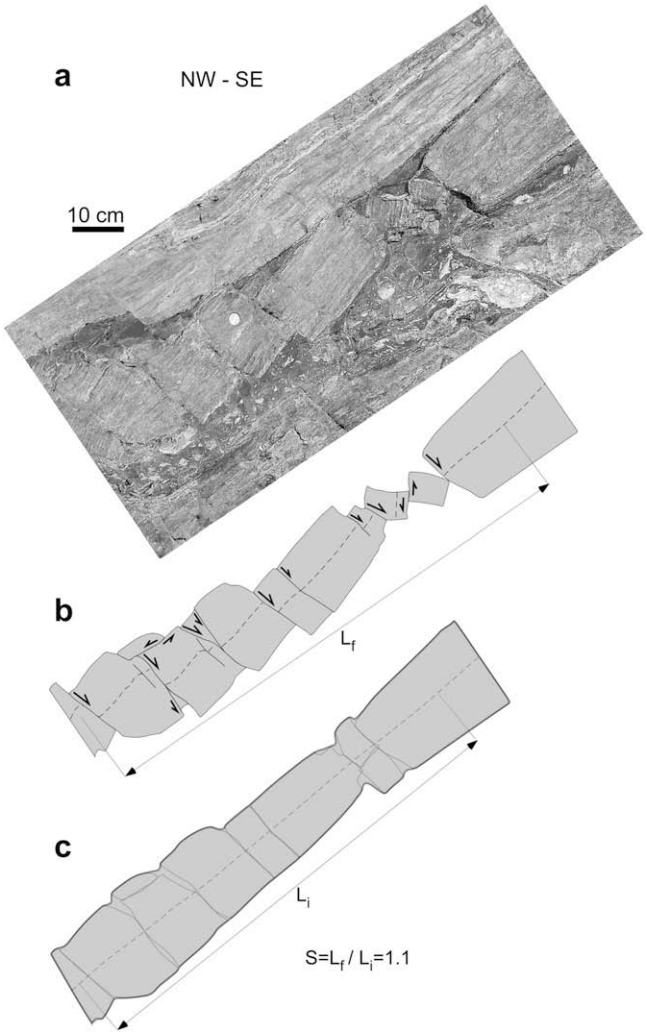

Fig. 6. Boudin train of metapsammite embedded in a brecciated marble, with boudins delimited by an E-down set of fractures. (a) Field photograph (see Fig. 4 for location). (b) Interpretative sketch with measured finite length (L_f). (c) Sketch of the layer reconstruction before fracturing, with measure of initial length (L_i) and stretch ($S = 1.1$, equal to the values obtained from the neighbouring trains in Fig. 5). Notice that the two small boudins on the right formed by rotation of a former single boudin and subsequent interlayer slip.

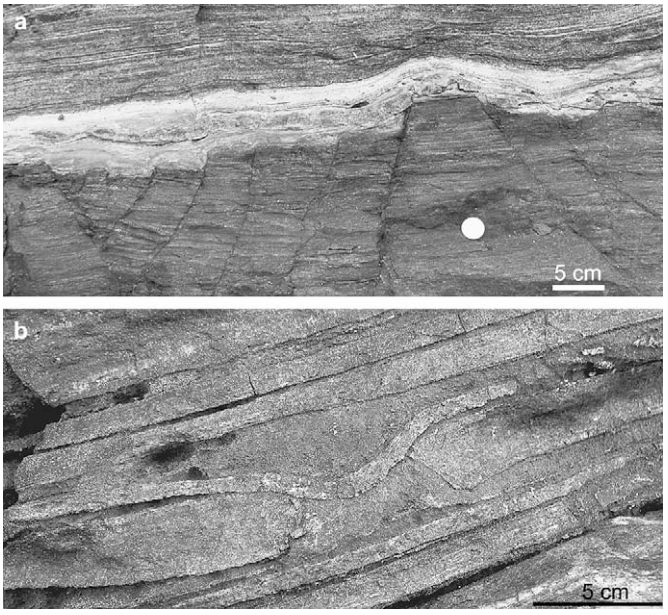

Fig. 7. Examples of different fracture types in the competent units. (a) Extensional conjugate faults giving rise to horst-and-graben arrays along the upper margin of a metapsammite bed. Note that in the marbles (above in the photograph) the displacement is accommodated by ductile flow. (b) Extension fracture boudinage in a metapsammitic layer. Notice the slight bending of the boudin corners and lack of parallelism of boudin walls, together with the bending and incipient cracking of the overlaying thinner layers. See Fig. 4 for location of the photographs.

Assuming that, in brittlely deforming rocks, σ_2 is parallel to the intersection between conjugate faults and σ_1 bisects the acute angle, it follows that the inferred local stress field for the competent layers is as shown in Fig. 4d. σ_2 and σ_3 are close to the layering plane, with σ_3 sub-parallel to the L_3 stretching lineation. Thus, fracture orientation and fabrics are compatible with a single (D_3) deformation event. The inferred σ_1 is not normal to the plane of mean layering but makes an angle of 75–80°. Lets now assume that the D_3 shear plane is parallel to layering (a reasonable assumption for multilayered rocks with a strong competence contrast). In the case of coaxial deformation, σ_1 would be normal to the shear plane. In the brittle layers from the study case, the deduced small deviation may indicate pure shear dominated transpression with a minor component of layer-parallel sinistral (top-to-the-north) shear.

If we do not consider the competent rocks individually, but as a boudinaged brittle layer embedded in a more ductile matrix, the bulk kinematics of the brittle–ductile system will be different to that assessed above. To address this, we applied the numerical approach of Passchier and Druguet (2002), based on the comparison of the relative displacements along synthetic- and antithetic-slip boudins embedded in a ductile matrix. The boudins in Figs. 5 and 6 were measured for this purpose. The obtained estimation confirms the sinistral (top-to-the-north) shear sense, but gives a degree of vorticity for the "boudins of psammite in marble" system much closer to simple shear (Wk ≈ 0.9). Consequently, a strong vorticity partitioning accompanies the partitioning in deformation mode (brittle vs. ductile), in accordance with the flow partitioning model of Lister and Williams (1983). This is a consequence of the strong refraction of the principal stress axes across layers with high competence contrast, as theoretically established by Stromgard (1973), Treagus (1973) and Mancktelow (1993). We can presume that the bulk flow regime for the overall 1–3 m scale multilayer unit would also be close to sinistral simple shear.

3.1.2. Structures related to layer-parallel shortening

F_3 folds associated with contractional deformation within the MMU are present in both competent and incompetent lithologies (Figs. 3b, 10 and 11) although they are best developed in the carbonate-rich layers. They display a wide variety of orientations and geometries, ranging from open to close to isoclinal. F_3 fold hinges typically plunge gently towards the north and east, and collectively form a girdle distribution that extends over an arc of 180° on stereographic projections (Figs. 2d and 4e). Asymmetric F_3 folds with hinges oblique to, and locally folding the L_3 stretching lineation systematically exhibit west vergence compatible with sinistral (or top-to-the-NW) shearing (Fig. 10). Fold asymmetry is better marked in the layered marbles. The associated F_3 fold axial planes are also highly variable, but typically dip gently to moderately towards the E and SE (Figs. 2d and 4).

Within individual F_3 fold trains, upright folds (relative to layering) display open to close geometries, while overturned folds are tight to isoclinal (Fig. 10d). In addition, individual fold hinges on the transport parallel sections may display more than 90° of hinge-

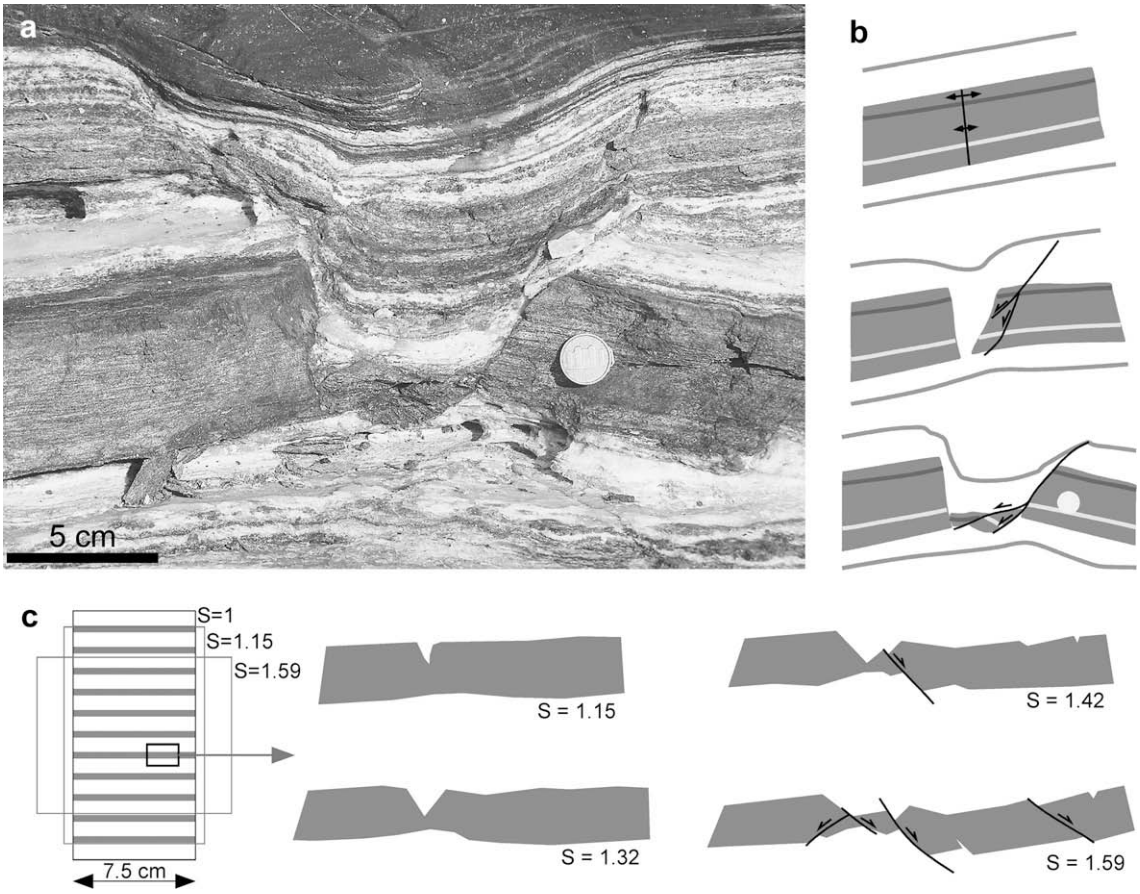

Fig. 8. Examples of the evolution from a wedge-shaped extension fracture into a shear fracture system. (a) Field photograph from the eastern slope of Clot de la Vellosa (see Fig. 4 for location). (b) Schematic interpretation of (a) through three deformation stages. (c) Sketches of four stages of an analogue experiment with layers of plasticine (from the company Oclu-Plast S.A., Barcelona) deformed under pure shear, layer-normal compression using the BCN-Stage. White is incompetent, grey competent. Thickness ratio of brittle to ductile layers: $T_r = 0.5$. S refers to bulk stretch value at each stage. First a wedge-shaped tension crack nucleates in a strong layer and this propagates into the incompetent layers as conjugate shear fractures and shear bands.

line curvature to define sheath fold geometries. Cross sections across the noses of such sheath folds display cats-eye fold patterns consistent with overall general shear involving a flattening component (see Alsop and Holdsworth, 2006; Alsop et al., 2007 for technique). However, not all folds which are parallel to the L_3 lineation display intense curvilinear hinge geometries. Some transport sub-parallel folds (with hinges within 15° of L_3) are marked by open to close interlimb angles and axial planes markedly oblique (30–45°) to foliation. These geometric relationships suggest that these folds nucleated in (rather than rotated into) a transport parallel orientation.

The presence in the MMU of extreme rheological contrasts between metapsammites or calc-silicate layers and marbles obviously promotes partitioning and will also encourage local ductile detachments between units. Such variable displacement patterns will trigger the generation of flow perturbation folds in which hinges may nucleate and form at high angles or even sub-parallel to transport (Alsop and Holdsworth, 2007). Locally preserved "fish hook" refold patterns indicate sequential development and rotation of folds during the overall progressive D_3 deformation. In addition, the hinges of adjacent folded layers may locally detach (along weak detachments) and rotate in a consistent sense relative to one another to create highly asymmetric fold geometries verging in the direction of top-to-the-west or sinistral shear (Fig. 10b). Such fold trains are clearly bounded by detachments, further supporting the flow perturbation model for the development of these folds.

In summary, the observed variation in fold geometries within the MMU suggests that folds may have nucleated at a variety of angles to the L_3 lineation, and in most cases have subsequently undergone a significant degree of rotation towards the flow direction during progressive D_3 deformation.

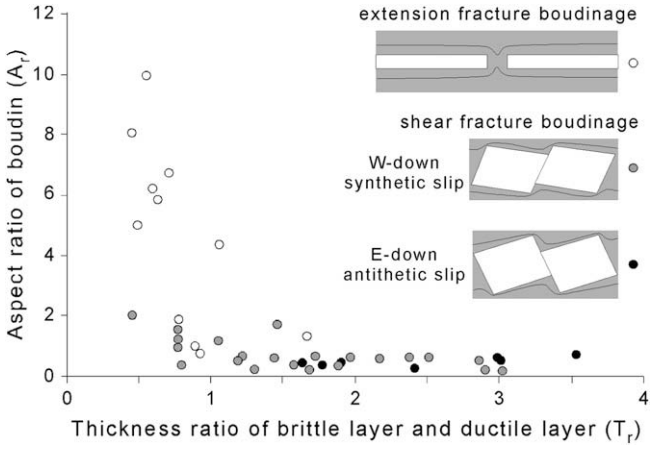

Fig. 9. Graph of the relationship between T_r and A_r parameters (Mandal et al., 2000) measured in the boudinaged layers of the study area.

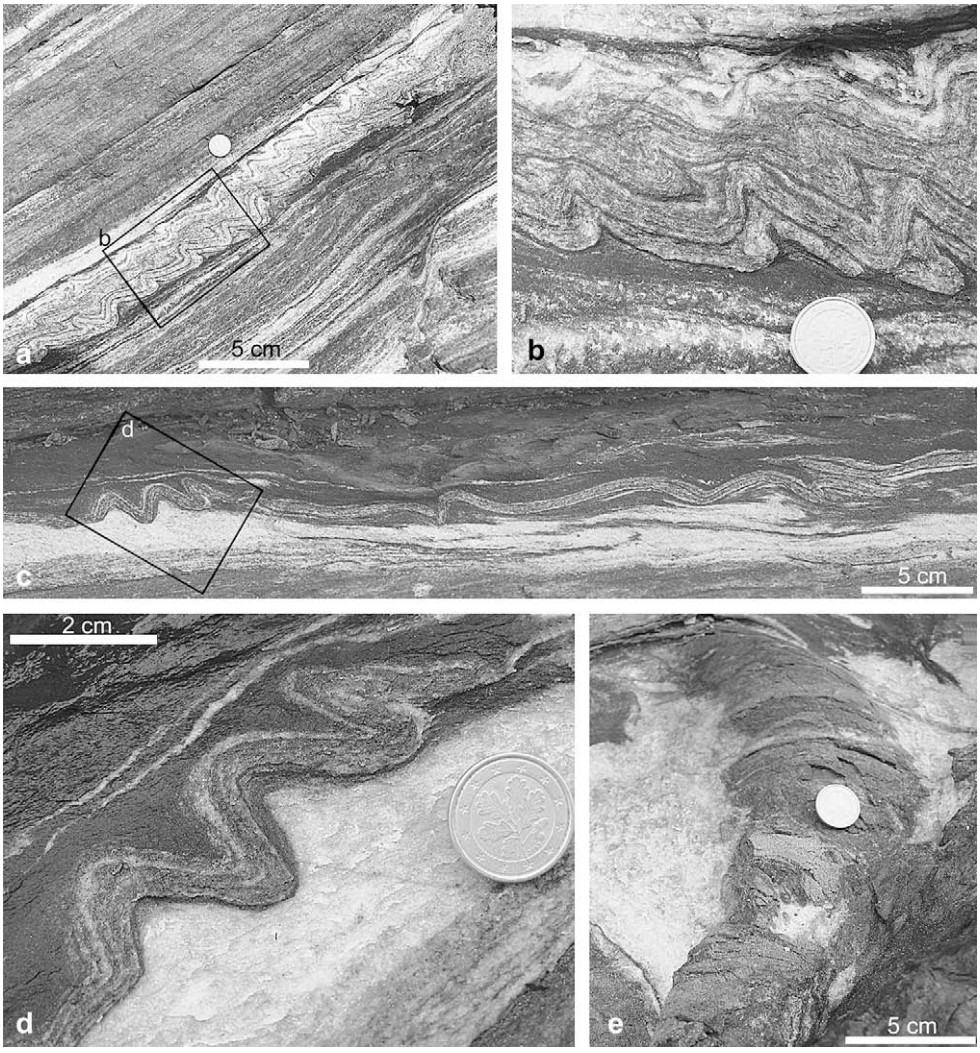

Fig. 10. Photographs of folding and related structures from the outcrops located on the eastern slope of Clot de la Vellosa (transport parallel section). (a) Asymmetric F_3 folds in layered marbles exhibiting west (left) vergence compatible with sinistral shearing. (b) Detail of (a) showing detachment and rotation of fold hinge zones. (c) Irregular folding and local thrusting along a competent, calc-silicate layer embedded in marbles. (d) Detail of (c) showing the progressive tightening of folds with overturning. (e) Curved F_3 fold hinge in marble with hinges oblique to, and folding, the L_3 stretching lineation. See Fig. 4 for location of photographs (a)–(d).

Heterogeneous deformation also takes place longitudinally along the layering (i.e. longitudinal strain partitioning), the layers being subjected to simultaneous local shortening and stretching in one direction (Fig. 1b) due to slight differences in the orientation of the layers (Carreras et al., 2005). In this way, folds with different geometry may develop along a competent layer, but also the layer can be segmented due to local thrusting (Fig. 10c) or boudinage (Fig. 11a and b). According to Mancktelow (2008b), the tendency for a layer in extension to fracture while the same layer in shortening folds can be explained in terms of the difference in mean stress or "tectonic pressure". Such a deformation pattern can be observed in transport parallel (Fig. 10c) and transport oblique sections (Fig. 11). The resulting pattern looks particularly complex and chaotic along sections at a high angle to transport direction, where blocks of competent rocks are "floating" in the extremely ductile marble (Fig. 11).

3.2. Marginal structures

Distinct structures are developed at the margins of the MMU related to the coupling between deformation styles inside and outside the unit. The two main sets of D_3 discrete shear zones developed in the schists locally merge with the MMU, resulting in ductile accommodation structures within the marbles. The steeply dipping set of shear zones with dextral movement prevails in the outcrops east of Clot de la Vellosa (Figs. 12a and 13a), whereas the shallowly-dipping set associated with top-to-the-south movement is more widespread west of Clot de la Vellosa (Figs. 12b and 13a). In all cases the discrete shears may cause local thickening of the MMU into wedge-shaped units, where the carbonate flows to "fill" space being created by the kinematics of the external D_3 shear zones (Figs. 12 and 13). The discrete D_3 shear zones in the schists are replaced in the immediately adjacent and more ductile MMU with broader zones of deformation and flow. The resulting accommodation folds are analogous to those observed at a smaller size in the marbles adjacent to interboudin fractures in competent layers within the MMU (Fig. 5).

The hinges of the accommodation folds are typically NE to SE trending with variably oriented axial planes reflecting the orientation of the D_3 shears. The D_3 accommodation folds locally refold early folds (Fig. 12b) and L_3 mineral lineation within the carbonates, as well as the local F_3 folds related to layer-parallel shortening

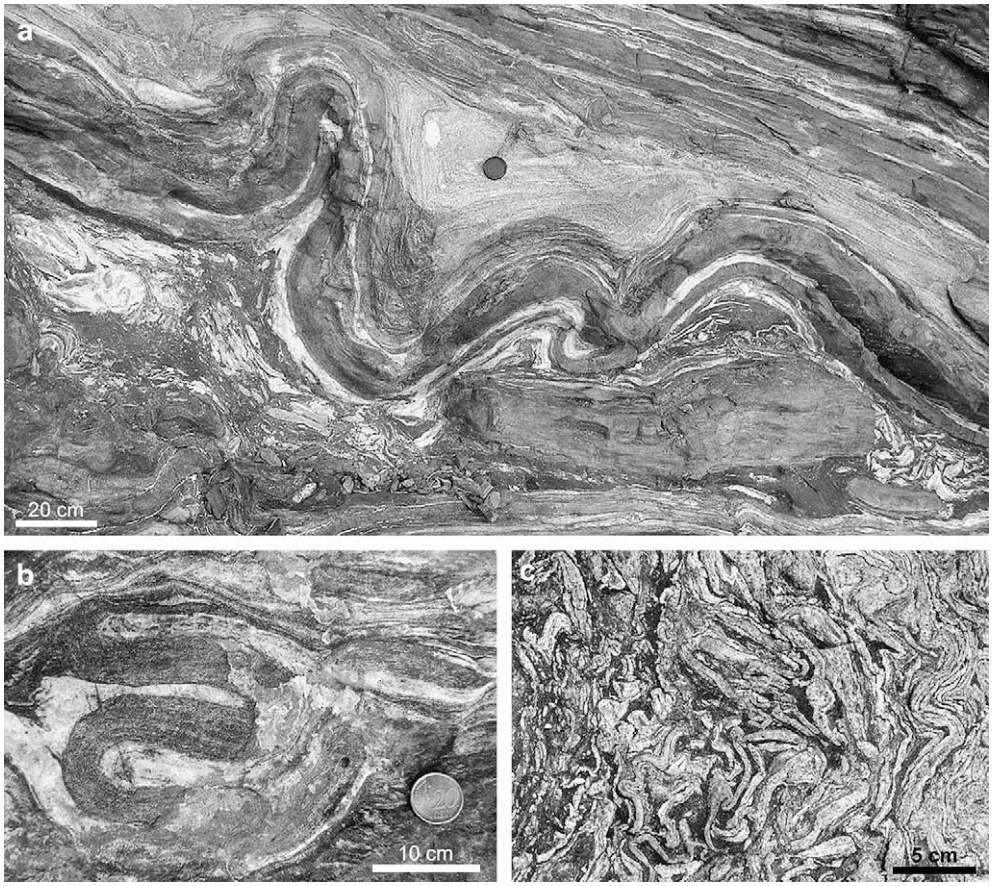

Fig. 11. Photographs of complex structures developed inside the MMU, observed along transport oblique sections (west of Clot de la Vellosa). (a) Disharmonic folds and boudin blocks of competent layers (metapsammite) embedded in extremely ductile marble with interference fold patterns. (b) Fold disruption and boudinage in a calc-silicate layer embedded in marble. Note the concentricity of folds, indicative of a high competence contrast. (c) Extremely complex folding pattern in interlaminated marble and calc-silicate rocks (section is approximately normal to transport).

(described above). These relationships suggest a complex and progressive deformation during the protracted D_3 event. Thus the MMU is accommodating layer-parallel shortening as well as external D_3 shears developed at a high angle to layering.

4. Interpretation

The described structures are interpreted to be the result of a progressive deformation sequence initiating under high-grade metamorphic conditions (D_2) and evolving towards medium- and low-grade metamorphic conditions (D_3).

In general, in the Cap de Creus Northern shear belt deformation localizes along D_3 shear zones (which are generally oblique to previous structures). Most of the shear zones have a dextral shear sense and all of them are compatible with an overall dextral transpression (Carreras, 2001). In the analysed zone, localization additionally occurs in rheologically weak materials (i.e. marbles) leading to further complexity in the area. Deformation partitioning in the case study took place at least at two different scales, one is internal and within the MMU, whilst the other is between the MMU and the adjacent rocks.

4.1. Centimetre to metre scale partitioning of the internal MMU

Before the onset of D_3, deformation is interpreted as rather homogeneous, as indicated by the presence of high-temperature D_2 fabrics in the metapsammites. However, the decrease in temperature during D_3 favours an increase in strength of the metapsammites (and calc-silicate rocks), increasing the competence contrast with respect to the marbles. The metapsammite and calc-silicate layers give large values of competence contrast with respect to the embedding marbles (the average competence contrast between metapsammite and marble is ≈ 100, and between calc-silicate rocks and marble is ≈ 50). Deformation gradually localizes along the incompetent rocks of the multilayer, with strong strain partitioning resulting in buckle folds and fractures in competent metapsammites and ductile accommodation structures in marbles. Particular features in this rheologically complex unit are (Fig. 13b):

(a) Partitioning of deformation mode: dominance of fractures over folds in strong layers and ductile flow (shearing and complex folding) in weak layers under overall ductile deformation conditions.
(b) Partitioning of strain magnitude: high strain in ductile layers and low strain in adjacent brittle rocks.
(c) Kinematic partitioning: non-coaxial dominated deformation prevails in ductile zones (indicated by the strong sinistral asymmetry of folds in the carbonate-rich layers and deformation of marbles which accommodate most of the layer-parallel shearing), whereas coaxial dominated deformation governs the brittle layers, as denoted by the orientation of extension and shear fractures in the metapsammites.

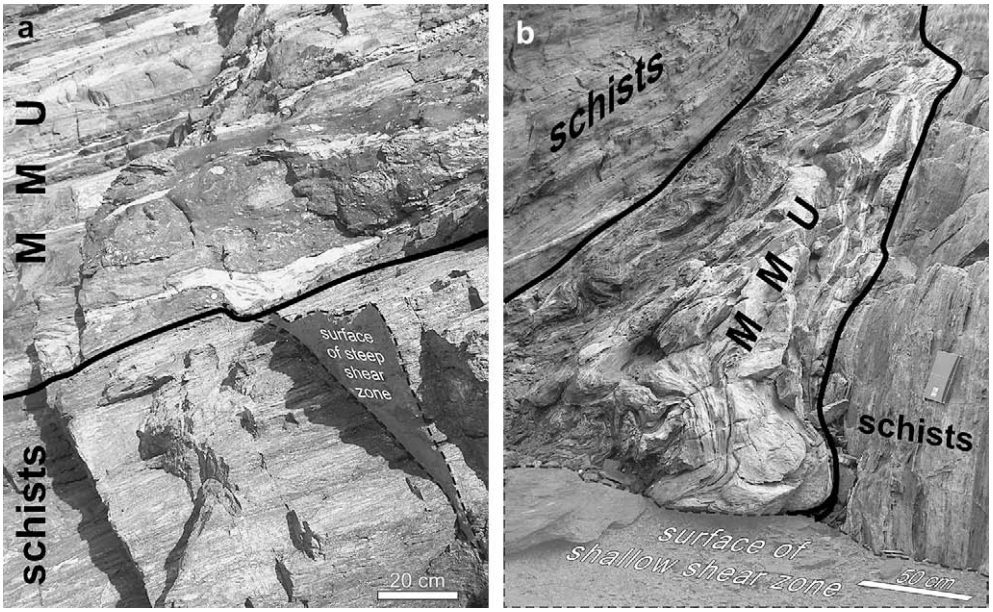

Fig. 12. Photographs of accommodation folds developed in marbles at the margins of the MMU where this is intersected by discrete D_3 shear zones in the adjacent schists. (a) The case of a steep shear zone from the east Clot de la Vellosa outcrops. (b) The case of a shallow shear zone from the west Clot de la Vellosa outcrops.

(d) Longitudinal partitioning: apart from the layer-transverse partitionings of points (a)–(c) above, a longitudinal partitioning is also observed and this is likely controlled by the heterogeneity of flow.
(e) Despite the noticeable differences mentioned above, the kinematics of the whole marble–metapsammite multilayer is compatible with a bulk layer-parallel sinistral–normal movement (Fig. 13).

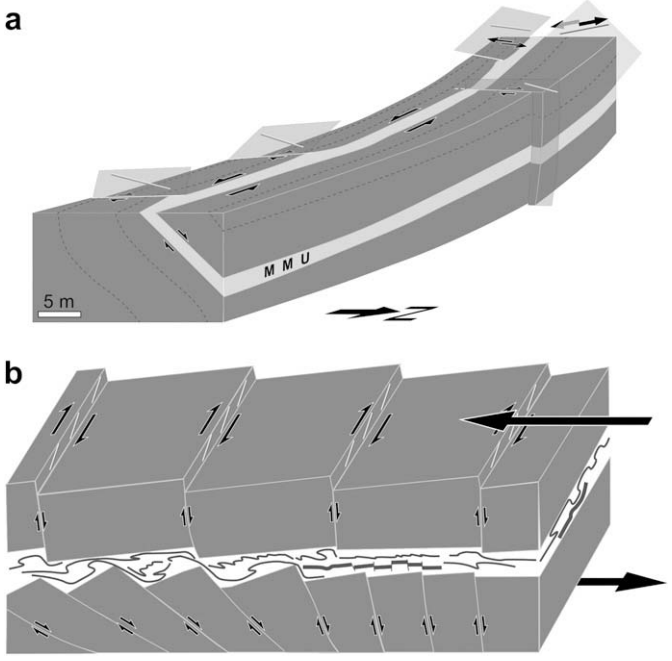

Fig. 13. Interpretative three-dimensional schematic diagrams of the structural patterns in the study area. The blocks are oriented with regard to the geographical coordinate system (a) and with regard to the kinematic axes of the MMU (b).

4.2. Decametric-scale partitioning between the MMU and the outer migmatitic schists

The complex structures observed inside the MMU contrast strongly with the relatively simple structures (D_2 transposition foliation locally cut by discrete D_3 shear zones) observed in the surrounding migmatitic schists (Fig. 13b). The differences between the two structural patterns can be attributed to deformation partitioning triggered by the rheological contrast during D_3 between rocks in the MMU multilayer and the surrounding migmatites.

This higher-order deformation partitioning has a particular significance for the interpretation of regional D_3 kinematics. As already stated, the structural pattern observed in the MMU is consistent with a layer-parallel sinistral–normal sense of shear (Fig. 13a), hence indicating "local" extensional tectonics. This is in apparent contradiction with the regional D_3 kinematics interpreted as a dextral transpression (Carreras, 2001). This apparent inconsistency can be simply solved by again taking account of the rheological decoupling between the MMU multilayer and the more homogeneous migmatites. In this case, the bulk regional dextral transpression is partitioned into (i) shear zones of predominantly dextral shear sense localised in rather homogeneous schistose domains and (ii) layer-parallel sinistral flow in a multilayer sequence (Fig. 14). The brittle–ductile behaviour inferred for the shear zones in the migmatitic schists (Fusseis et al., 2006; Fusseis and Handy, 2008) would not be directly related to strain partitioning, but most likely caused by cyclic variations in strain rate (Fusseis et al., 2006; Fusseis and Handy, 2008; Mancktelow, 2008a). The initial anisotropy (S_2) would be the same in both the MMU and the adjacent schists, but the strong rheological contrast in the MMU would have triggered the layer-parallel sinistral flow.

This setting is not unique in the evolution of the transpressional tectonics in Cap de Creus, as an apparent contradiction was also found related to the previous D_2 event between sinistral shearing (based on kinematic analysis at the metric scale structures) and dextral shearing on a regional scale (Carreras and Druguet, 1994; Druguet et al., 1997). In that case, partitioning of strain was controlled by the pre-existing anisotropy though no evidence of

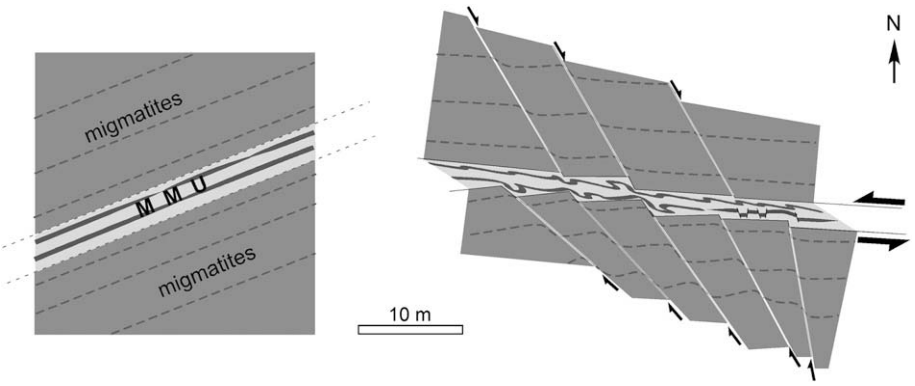

Fig. 14. Sketches showing the structural evolution of the case study (before and after the D_3 deformation event) in which bulk non-coaxial deformation is partitioned between highly contrasting lithological units in mode of deformation (brittle–ductile), strain magnitude (high strain vs. low strain), vorticity (pure shear dominated vs. simple shear dominated) and kinematics (dextral–sinistral).

a strong lithological/rheological contrast was found such as in the present study. From a comparable situation, Pennacchioni and Mancktelow (2007) also proved that kinematic partitioning is determined by the orientation of pre-existing discontinuities relative to the bulk flow.

5. Conclusions

This case study illustrates extreme deformation partitioning in the Cap de Creus shear belt which is interpreted to be the result of strong rheological heterogeneities accentuated by a gradual decrease in temperature of the deforming rocks (greenschist-facies, retrograde metamorphic conditions). A multilayer of contrasting incompetent and competent lithologies (marble–metapsammite unit, MMU) exhibits mostly ductile (folding) and brittle (boudinage) structures respectively. The MMU itself also represents a detachment level within the relatively rigid and rather monotonous strongly recrystallized migmatitic schists (Figs. 13 and 14). These schists are marked by the development of sets of discrete shear zones. Complex patterns arise at the boundaries of the MMU (i.e. wedge-shaped zones of accommodation folds) due to the interaction between brittle–ductile shear zones affecting the migmatites and ductile flow of the incompetent marbles.

Deformation partitioning is exemplified at different scales (centimetric to decametric), directions (longitudinal and transverse with respect to layering) and levels (with partitioning of deformation mode, strain magnitude, vorticity and kinematics). In all cases, partitioning is influenced by the strong rheological contrast. In particular, this case study is a paradigm of how, as a result of strain partitioning induced by rheological variations and by the specific orientation of the anisotropy planes, local kinematics may be entirely opposite to bulk kinematics so that analysis of structures in a given domain might lead to interpretations in apparent contradiction with the bulk regional kinematics. Consequently, caution is needed when making regional tectonic interpretations from meso- (and micro) structures developed in rheologically highly inhomogeneous domains. This study therefore demonstrates the importance of integrated multiscale structural analyses, because kinematic inferences based on separate analyses at the layer, outcrop and regional scales may differ significantly.

Acknowledgements

This work was funded by the Spanish Ministry of Education and Science (Project CGL2007-66857-C02-01). We thank Lina M. Castaño for support in both field and laboratory work and the referees, Florian Fusseis and Neil Mancktelow for their constructive reviews.

References

Alsop, G.I., Carreras, J., 2007. Structural evolution of sheath folds: a case study from Cap de Creus. Journal of Structural Geology 29, 1915–1930.
Alsop, G.I., Holdsworth, R.E., 2006. Sheath folds as discriminators of bulk strain type. Journal of Structural Geology 28, 1588–1606.
Alsop, G.I., Holdsworth, R.E., 2007. Flow perturbation folding in shear zones. In: Ries, A.C., Butler, R.W.H., Graham, R.D. (Eds.), Deformation of the Continental Crust: the legacy of Mike Coward. Geological Society, London, Special Publications, vol. 272, pp. 77–103.
Alsop, G.I., Holdsworth, R.E., McCaffrey, K.J.W., 2007. Scale invariant sheath folds in salt, sediments and shear zones. Journal of Structural Geology 29, 1585–1604.
Bons, P.D., Druguet, E., Hamann, I., Carreras, J., Passchier, C.W., 2004. Apparent boudinage in dykes. Journal of Structural Geology 26, 625–636.
Carreras, J., 2001. Zooming on Northern Cap de Creus shear zones. Journal of Structural Geology 23, 1457–1486.
Carreras, J., Casas, J.M., 1987. On folding and shear zone development: a mesoscale structural study on the transition between two different tectonic styles. Tectonophysics 135, 87–98.
Carreras, J., Druguet, E., 1994. Structural zonation as a result of inhomogeneous non-coaxial deformation and its control on syntectonic intrusions: an example from the Cap de Creus area (eastern-Pyrenees). Journal of Structural Geology 16, 1525–1534.
Carreras, J., Ramírez, J., 1984. The geological significance of the Port de la Selva Gneisses (Eastern Pyrenees, Spain). In: Sassi, F.P., Julivert, M. (Eds.), I.G.C.P. N°5 Newsletter 6, pp. 27–31.
Carreras, J., Druguet, E., Griera, A., 2005. Shear zone-related folds. Journal of Structural Geology 27, 1229–1251.
Castiñeiras, P., Navidad, M., Liesa, M., Carreras, J., Casas, J.M., 2008. U–Pb zircon ages (SHRIMP) for Cadomian and Early Ordovician magmatism in the Eastern Pyrenees: new insights into the pre-Variscan evolution of the northern Gondwana margin. Tectonophysics 461, 228–239.
Druguet, E., 1997. The Structure of the NE Cap de Creus Peninsula. Relationships with Metamorphism and Magmatism. Unpublished thesis. Universitat Autònoma de Barcelona.
Druguet, E., 2001. Development of high thermal gradients by coeval transpression and magmatism during the Variscan orogeny: insights from the Cap de Creus (Eastern Pyrenees). Tectonophysics 332, 275–293.
Druguet, E., Carreras, J., 2006. Analogue modelling of syntectonic leucosomes in migmatitic schists. Journal of Structural Geology 28, 1734–1747.
Druguet, E., Passchier, C.W., Carreras, J., Victor, P., den Brok, S., 1997. Analysis of a complex high-strain zone at Cap de Creus, Spain. Tectonophysics 280, 31–45.
Druguet, E., Czeck, D.M., Carreras, J., Castaño, L.M., 2008. Emplacement and deformation features of syntectonic leucocratic veins from Rainy Lake zone (Western Superior Province, Canada). Precambrian Research 163, 384–400.
Fusseis, F., Handy, M.R., 2008. Micromechanisms of shear zone propagation at the brittle–viscous transition. Journal of Structural Geology 30, 1242–1253.
Fusseis, F., Handy, M.R., Schrank, C., 2006. Networking of shear zones at the brittle-to-viscous transition (Cap de Creus, NE Spain). Journal of Structural Geology 28, 1228–1243.
Ghosh, S.K., 1994. Structural Geology: Fundamental and Modern Developments. Pergamon Press, London.
Gómez-Rivas, E., Bons, P.D., Griera, A., Carreras, J., Druguet, E., Evans, L., 2007. Strain and vorticity analysis using small-scale faults and associated drag folds. Journal of Structural Geology 29, 1882–1899.
Grujic, D., Mancktelow, N.S., 1995. Folds with axes parallel to the extension direction: an experimental study. Journal of Structural Geology 17, 279–291.

Harris, L.B., Koyi, H.A., Fossen, H., 2002. Mechanisms for folding of high-grade rocks in extensional tectonic settings. Earth-Science Reviews 59, 163–210.
Healy, D., Jones, R.R., Holdsworth, R.E., 2006. Three-dimensional brittle shear fracturing by tensile crack interaction. Nature 439, 64–67.
Hippertt, J., Tohver, E., 1999. On the development of zones of reverse shearing in mylonitic rocks. Journal of Structural Geology 21, 1603–1614.
Hutton, D.H.W., 1982. A tectonic model for the emplacement of the main Donegal granite. Journal of the Geological Society, London 139, 615–631.
Ishii, K., 1992. Partitioning of non-coaxiality in deforming layered rock masses. Tectonophysics 210, 33–43.
Jiang, D., 1994. Flow variation in layered rocks subjected to bulk flow of various kinematic vorticities: theory and geological implications. Journal of Structural Geology 16, 1159–1172.
Jones, R.R., Tanner, R.P.G., 1995. Strain partitioning in transpression zones. Journal of Structural Geology 17, 793–802.
Lin, S., Jiang, D., Williams, P.F., 2007. Importance of differentiating ductile slickenside striations from stretching lineations and variation of shear direction across a high-strain zone. Journal of Structural Geology 29, 850–862.
Lister, G.S., Williams, P.F., 1983. The partitioning of deformation in flowing rock masses. Tectonophysics 92, 1–23.
Mancktelow, N.S., 1993. Tectonic overpressure in competent mafic layers and the development of isolated eclogites. Journal of Metamorphic Geology 11, 801–812.
Mancktelow, N.S., 2008a. Interaction between brittle fracture and ductile flow during crustal deformation. Bollettino della Società Geologica Italiana (Italian Journal of Geoscience) 127, 217–220.
Mancktelow, N.S., 2008b. Tectonic pressure: theoretical concepts and modelled examples. Lithos 103, 149–177.
Mandal, N., Chakraborty, C., Samanta, S.K., 2000. Boudinage in multilayered rocks under layer-normal compression: a theoretical analysis. Journal of Structural Geology 22, 373–382.
Navidad, M., Carreras, J., 1995. Pre-Hercynian magmatism in the Eastern Pyrenees (Cap de Creus and Albera Massifs) and its geodynamical setting. Geologie en Mijnbouw 74, 65–77.
Passchier, C.W., 1990. Reconstruction of deformation and flow parameters from deformed veins sets. Tectonophysics 180, 185–199.
Passchier, C.W., Druguet, E., 2002. Numerical modeling of asymmetric boudinage. Journal of Structural Geology 24, 1789–1803.
Peacock, D.C.P., Sanderson, D.J., 1992. Effects of layering and anisotropy on fault geometry. Journal of the Geological Society, London 149, 793–802.
Pennacchioni, G., Mancktelow, N.S., 2007. Nucleation and initial growth of a shear zone network within compositionally and structurally heterogeneous granitoids under amphibolite facies conditions. Journal of Structural Geology 29, 1757–1780.
van der Pluijm, B.E., Marshak, S., 2004. Earth Structure: an Introduction to Structural Geology and Tectonics, second ed. W.W. Norton, New York, 656 pp.
Ramberg, H., 1955. Natural and experimental boudinage and pinch- and swell structures. Journal of Geology 63, 512–526.
Ramsay, J.G., 1982. Rock ductility and its influence on the development of tectonic structures in mountain belts. In: Hsu, K.J. (Ed.), Mountain Building Processes. Academic Press, London, pp. 111–127.
Schmalholz, S.M., Podladchikov, Y.Y., 2001. Strain and competence contrast estimation from fold shape. Tectonophysics 340, 195–213.
Schmid, D.V., Podladchikov, Y.Y., 2006. Fold amplification rates and dominant wavelength selection in multilayer stacks. Philosophical Magazine 86, 3409–3423.
Schöpfer, M.P.J., Childs, C., Walsh, J.J., 2006. Localisation of normal faults in multilayer sequences. Journal of Structural Geology 28, 816–833.
Stearns, D.W., 1964. Macrofracture patterns on Teton Anticline, Northwest Montana. American Geophysical Union Transactions 45, 107–108.
Strachan, L.J., Alsop, G.I., 2006. Slump folds as estimators of palaeoslope: a case study from the Fisherstreet Slump of County Clare, Ireland. Basin Research 18, 451–470.
Stromgard, K.E., 1973. Stress distribution during formation of boudinage and pressure shadows. Tectonophysics 16, 215–248.
Suppe, J., 1985. Principles of Structural Geology. Prentice Hall, Englewood Cliffs, New Jersey, 537 pp.
Takeda, Y.-T., Griera, A., 2006. Rheological and kinematical responses to flow of two-phase rocks. Tectonophysics 427, 95–113.
Tikoff, B., Teyssier, C., 1994. Strain modeling of displacement-field partitioning in transpressional orogens. Journal of Structural Geology 16, 1575–1588.
Treagus, S.H., 1973. Buckling stability of a viscous single-layer system, oblique to the principal compression. Tectonophysics 19, 271–289.
Twiss, R.J., Moores, E.M., 1992. Structural Geology. W.H. Freeman, New York.
Vigneresse, J.L., Tikoff, B., 1999. Strain partitioning during partial melting and crystallizing felsic magmas. Tectonophysics 312, 117–132.
White, S., Burrows, S.E., Carreras, J., Shaw, N., Humphreys, J., 1980. On mylonites in ductile shear zones. Journal of Structural Geology 2, 175–187.
Zulauf, J., Zulauf, G., 2005. Coeval folding and boudinage in four dimensions. Journal of Structural Geology 27, 1061–1068.